Supporting Information:

High-pressure observation of elusive iodoplumbic acid in different hydronium-hydrate solid forms

Szymon Sobczak,[a] Athena M. Fidelli,[b] Jean-Louis Do[b], George Demopoulos*, [c] Audrey Moores*[b], Tomislav Friščić*[b] and Andrzej Katrusiak*[a]

[a]   S. Sobczak, Prof. A. Katrusiak, Departament of Chemistry, Adam Mickiewicz University, Poznan, Uniwersytetu Poznanskiego 8, 61-619 Poznan, Poland
[b]   Dr. Athena Fidelli, Prof. Tomislav Friščić, Department of Chemistry, McGill University, 801 Sherbrooke St. W., H3A 0B8 Montreal, Canada
[c]   Department of Materials Engineering, McGill University

General microscopy

For observing and controlling the growth of compounds **3**, **4** and β-PbI$_2$ single crystals, Olympus MVX10 microscope, equipped with MV PLAPO 1xFF objective was used, with a total optical magnification ranging from 4× to 80×, equipped with an Olympus Digital Camera SC 30/MVX-TV1XC. All crystal dimensions were measured with Olympus cellSens imaging software.

Pseudosymmetry in 1

Similarly as in SiC polytypes,[10] at least two structure can be found for the layered structure of **1**. Several independent single-crystal diffraction experiments have been made to identify the correct space group. Depending on the shift in the position of water molecules, occupying the interlayer space and arranged in a honeycomb formation, two different symmetries can be refined: monoclinic space group $C2/m$ (mC) and trigonal space group R-$3m$ (hR). However, the careful analysis of systematic absences suggests that the crystal belongs to mC group, which can be confused with the strained hexagonal lattice. This strain causes broadening of reflections along c^*, during the transformation from mC to hR leads to differentiation in the unit-cell parameters of about 0.04 Å and described by the matrix:

$$\begin{pmatrix} -1/2 & 0.5 & 0 \\ 0 & -1 & 0 \\ 1.5 & 0 & 3 \end{pmatrix} \begin{pmatrix} a_c \\ b_c \\ c_c \end{pmatrix} = \begin{pmatrix} a_r \\ b_r \\ c_r \end{pmatrix}$$

Where c and r indexes indicate mC to hR lattices, respectively.

High-pressure experiments

For each high-pressure experiment a liquid solution of PbI_2 dissolved in concentrated aqueous hydroiodic acid (HI, 57% by weight) was loaded to a modified Merrill-Bassett diamond anvil cell (DAC).[1] The DAC anvils were supported directly on the steel discs with conical windows (the culet size was 0.8 mm, type 1A diamonds, a steel gasket 0.15 mm thick, the hole diameter 0.45 mm).[2] Pressure in the DAC was determined by the ruby fluorescence (R1 ruby line) shift with a Photon Control spectrometer affording an accuracy of 0.02 GPa.[3,4]

The single-crystals of **3** and **4** were obtained in isochoric conditions: after the polycrystalline mass precipitated, the DAC with was heated using a hot-air gun till all but one grain melted. Then the single crystal grew as the DAC was cooled slowly to room temperature. Temperature inside DAC was determined using a dual-method approach: a laser thermometer directed at the diamond anvil's surface and a thermocouple mounted directly on the anvil. The high thermal conductivity of diamond ensured that the laser thermometer readings provide a reliable estimation of the DAC's internal temperature, which is cross-verified with the thermocouple measurements. The progress and experimental details on growing the single crystals of **3** and **4** are shown in Figures S1 and S2.
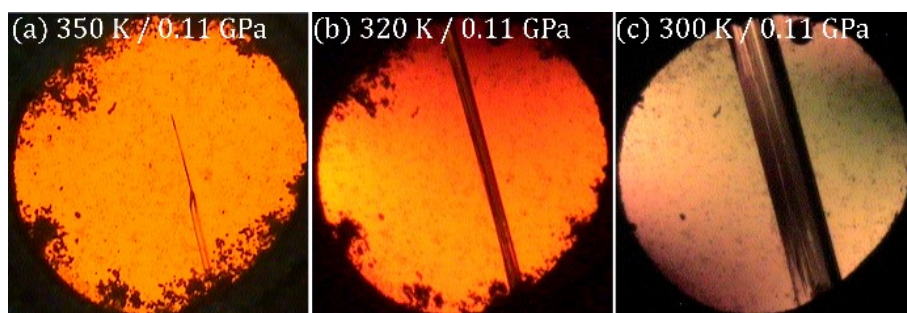
Figure S1. Single crystal of **3** grown *in situ* in a DAC in isochoric conditions at (a) 350 K; (b) 320 K and; (c) 300 K / 0.11 GPa. The ruby sphere for pressure calibration lies at the upper-right edge of the chamber
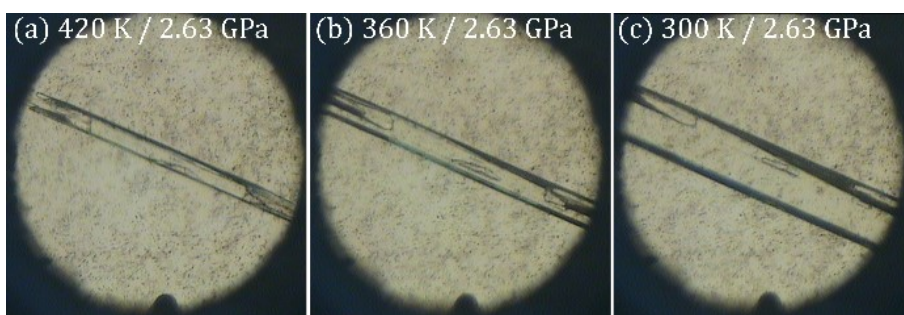
Figure S2. Single crystal of **4** grown *in situ* in a DAC in isochoric conditions at (a) 420 K; (b) 360 K and; (c) 300 K / 2.63 GPa. The ruby sphere for pressure calibration lies at the lower-edge of the chamber.

Single crystals of β-PbI$_2$ were obtained similarly to those of **3** and **4**, however due to the phase transformation at room temperature at 1.2 GPa, the single crystal grown at 2.05 GPa was kept at 320 K and the X-ray diffraction experiment was performed at this temperature. Temperature inside DAC was determined using a dual-method approach: a laser thermometer directed at the diamond anvil's surface and a thermocouple mounted directly on the anvil. The high thermal conductivity of diamond ensured that the laser thermometer readings provide a reliable estimation of the DAC's internal temperature, which is cross-verified with the thermocouple measurements.
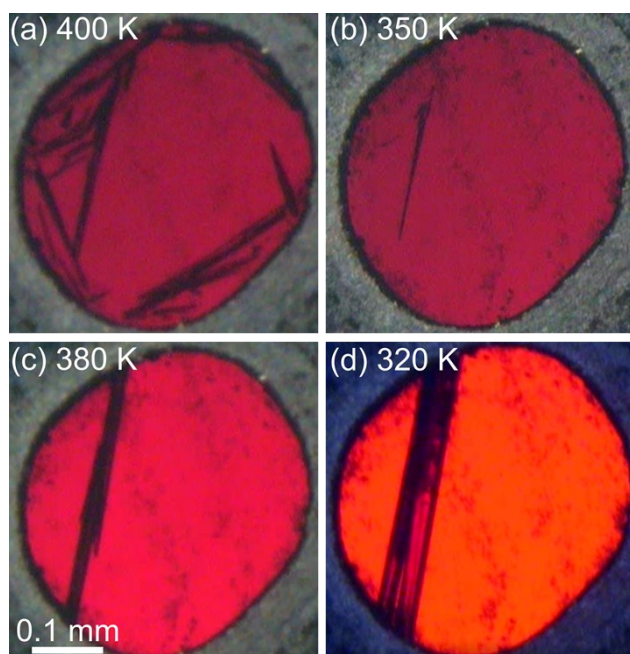
Figure S3. Isochoric growth (a-d) of the pink single-crystal of β-PbI$_2$ in the DAC at 2.05 GPa. The β-PbI$_2$ crystals display a reverse solubility phenomena resulting in crystal growth upon heating from 350 to 380 K.

Diffraction data were collected at 295 K for **1**, **3** and **4** and at 320 K for β-PbI$_2$, by using a KM-4 CCD diffractometer with the graphite-monochromated MoKα radiation. The DAC was centered by the gasket-shadow method.[5] The CrysAlisCCD and CrysAlisRED programs[6] were used for collecting the data, determination of the UB-matries, and for initial data reductions and Lp corrections. Reflection intensities were corrected for the DAC and sample absorption; the gasket shadowing and the reflections of diamond-anvils were eliminated.[7] All structures were solved by direct methods, and refined with anisotropic displacement parameters, with programs ShelXS and ShelXL[8] using Olex2 interface.[9] Details of structure refinements and crystal data are given in Table S1.

Table S1. Detailed crystallographic data for **1**, **3**, **4** and β-PbI$_2$

Compound	**1** $(H_3O)_{2-x}Pb_xI_2 \cdot (2-2x)H_2O$	**3** $(H_3O)PbI_3 \cdot 4H_2O$	**3** $(H_3O)PbI_3 \cdot 4H_2O$	**3** $(H_3O)PbI_3 \cdot 4H_2O$	**4** $(H_3O)PbI_3 \cdot 3H_2O$	β-PbI$_2$
CSD Number	**2071140**	**-**	**2071141**	**2071142**	**2071143**	**2071144**
Pressure	0.1 MPa	0.20 GPa	0.50 GPa	1.20 GPa	2.63 GPa	2.05 GPa
Temperature	300 K	300 K	300 K	300 K	300 K	320 K
Formula weight	227.79	667.89	667.89	667.89	651.89	691.48
Wavelength (Å)	0.71073	0.71073	0.71073	0.71073	0.71073	0.71073
Crystal system	monoclinic	monoclinic	monoclinic	monoclinic	monoclinic	monoclinic
Space group	*C2/c*	*I2/m*	*I2/m*	*I2/m*	*P2$_1$/m*	*C2/m*
Unit cell dimensions *a* (Å)	4.5598(3)	16.92(14)	16.205(2)	16.119(13)	9.57(3)	14.06(4)
b (Å)	11.1985(18)	4.4666(7)	4.51695(14)	4.5261(9)	4.513(3)	4.4260(12)
c (Å)	90	17.31(2)	17.184(14)	16.88(4)	12.98(11)	10.540(6)
Unit cell angles α (°)	118.023(19)	90.0	90	90	90	90
β (°)	90	112.0(4)	111.50(4)	111.25(17)	95.9(6)	93.08(12)
γ (°)	355.86(9)	90.0	90	90	90	90
Volume (Å^3)	1068.10(14)	1213(10)	1170.3(10)	1147(3)	558(5)	654.9(17)
Z/Z'	4/0.5	4/0.5	4/0.5	4/0.5	2/0.5	2/0.25
Molecular volume (*V/Z*)	267.025	303.25	292.575	286.75	279	327.45
Calculated density (g/cm^3)	4.252	3.657	3.791	3.866	3.883	7.013
Absorption (mm^{-1})	27.566	24.068	22.303	22.746	23.395	52.550
F(000)	383.0	-	1124.0	1124.0	546.0	1128.0
Crystal size (mm)	0.1 × 0.1 × 0.05	0.445 × 0.127 × 0.068	0.32 × 0.101 × 0.065	0.30 × 0.10 × 0.06	0.30 × 0.20 × 0.15	0.30 × 0.10 × 0.10
2θ-range for data collection (°)	8.246 to 57.384	7.0648 to 49.3486	5.404 to 52.382	8.758 to 51.294	4.28 to 55.116	3.87 to 52.736
Min/max indices: *h, k, l*	-10 ≤ h ≤ 10, -6 ≤ k ≤ 6, -15 ≤ l ≤ 15	-4 ≤ h ≤ 4, -5 ≤ k ≤ 5, -19 ≤ l ≤ 19	-19 ≤ h ≤ 19, -5 ≤ k ≤ 5, -5 ≤ l ≤ 5	-16 ≤ h ≤ 16, -5 ≤ k ≤ 5, -7 ≤ l ≤ 8	-10 ≤ h ≤ 8, -5 ≤ k ≤ 5, -8 ≤ l ≤ 6	-8 ≤ h ≤ 8, -5 ≤ k ≤ 5, -12 ≤ l ≤ 12
Reflect. Collected/unique	3208/523	8331/-	6503/335	1022/323	788/287	2000/258
Rint	0. 0541	0.2558	0.0592	0.1061	0.1665	0.2469
Refinement method			Full-matrix least-squares on F^2			
Completeness (%)	99.7	25.8	39.5	36.6	23.3	42.7
Data/restrains/parameters	523/0/21	-	335/0/42	323/6/42	287/39/38	258/17/29
Goodness-of-fit on F^2	1.019	-	0.857	1.035	0.962	1.067
Final R$_1$/wR$_2$ (I>2σ1)	0.0364 /0.0794	-	0.0329/0.0832	0.0773/ 0.1686	0.0851/0.2064	0.0818/0.1946
R$_1$/wR$_2$ (all data)	0.0492 /0.0877	-	0.0352/0.0853	0.1013/0.1834	0.2011/0.2788	0.1309/0.2211
Largest diff. peak/hole (e.Å^{-3})	2.72/-0.75	-	0.66/-0.55	0.88/-1.01	0.96/-1.02	2.77/-1.63

$w = 1/(\sigma^2 F_o^2 + w_1{}^2 * P^2 + w_2 * P)$, where $P = (Max(F_o^2, 0) + 2 * F_c^2)$

Ball-Milling experiments

Milling Synthesis of $[H_3O]_{2x}[Pb_{1-x}I_2]\cdot(2-2x)H_2O$ (**1**)

For the ball-milling synthesis, 0.461 g (1 mmol) of PbI_2 was added to one half of zirconia (ZrO_2) 10 mL jars, followed by the addition of 67 µL (0.5 mmol) of aqueous hydroiodic acid (HI 57%) and one 3.5 g zirconia ball. The jar was carefully sealed and placed on a MM400 mixer mill and the reaction mixture was milled for 30 minutes at an oscillation rate of 30 Hz. Reaction completion afforded a bright yellow product, which was left to dry in dark for 1h. The resulting solid product was scraped off the jar walls and subjected to powder X-ray diffraction (PXRD) analysis, revealing the formation of compound **1**. Compound **1** can be also isolated when performing the 1:1 stoichiometric reaction by milling 0.230 g (0.5 mmol) of PbI_2 with 67 µL (0.5 mmol) of aqueous hydroiodic acid (HI 57%), respectively.

Milling Synthesis of $(H_3O)_2Pb_3I_8\cdot6H_2O$ (**2**)

For the ball-milling synthesis 0.230 g (0.5 mmol) of PbI_2 was added to one half of zirconia (ZrO_2) 10 mL jars, followed by the addition of 201 µL (1.5 mmol) of aqueous hydroiodic acid (HI 57%) and one 3.5 g zirconia ball. The jar was carefully sealed and placed on a MM400 mixer mill and the reaction mixture was milled for 30 minutes at an oscillation rate of 30 Hz. Reaction completion afforded a bright yellow product, which was left to dry in dark overnight. The resulting product was scraped off the jar walls and subjected to powder X-ray diffraction (PXRD) analysis, revealing the formation of compound **2**.
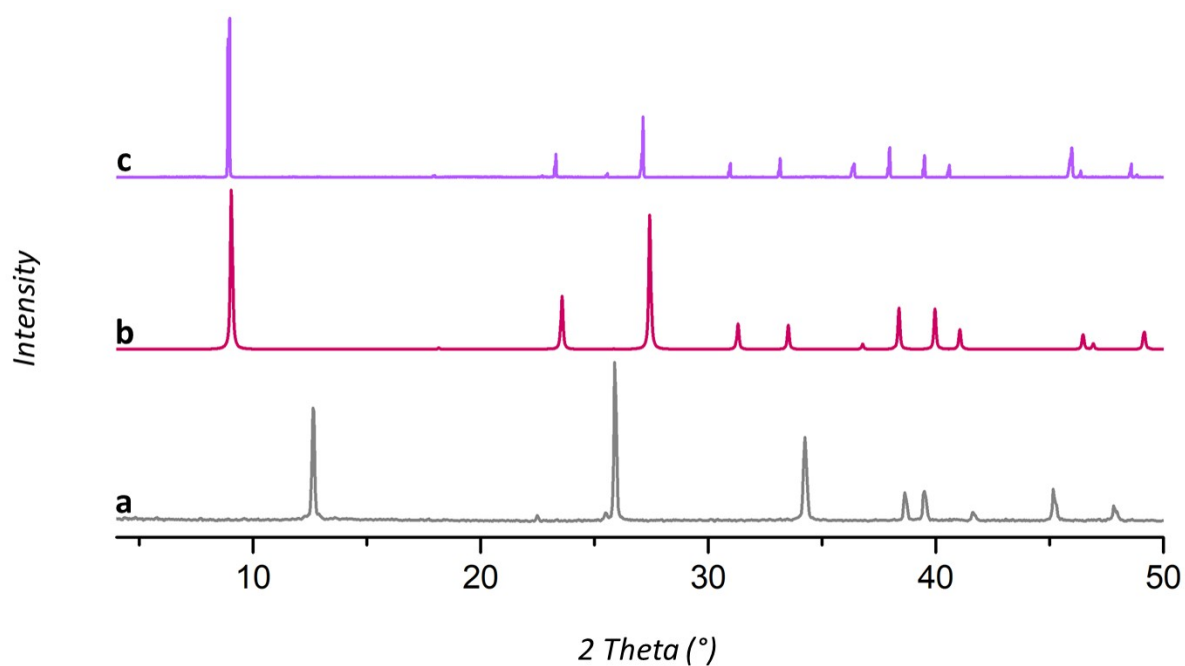
Figure S4. Powder X-ray diffraction patterns: a) experimental pattern of PbI_2 (Sigma Aldrich) b) simulated pattern of $[H_3O]_{2x}[Pb_{1-x}I_2] \cdot (2-2x)H_2O$ (**1**) and c) experimental pattern of the milling product from the $1.5PbI_2$:HI stoichiometric reaction.
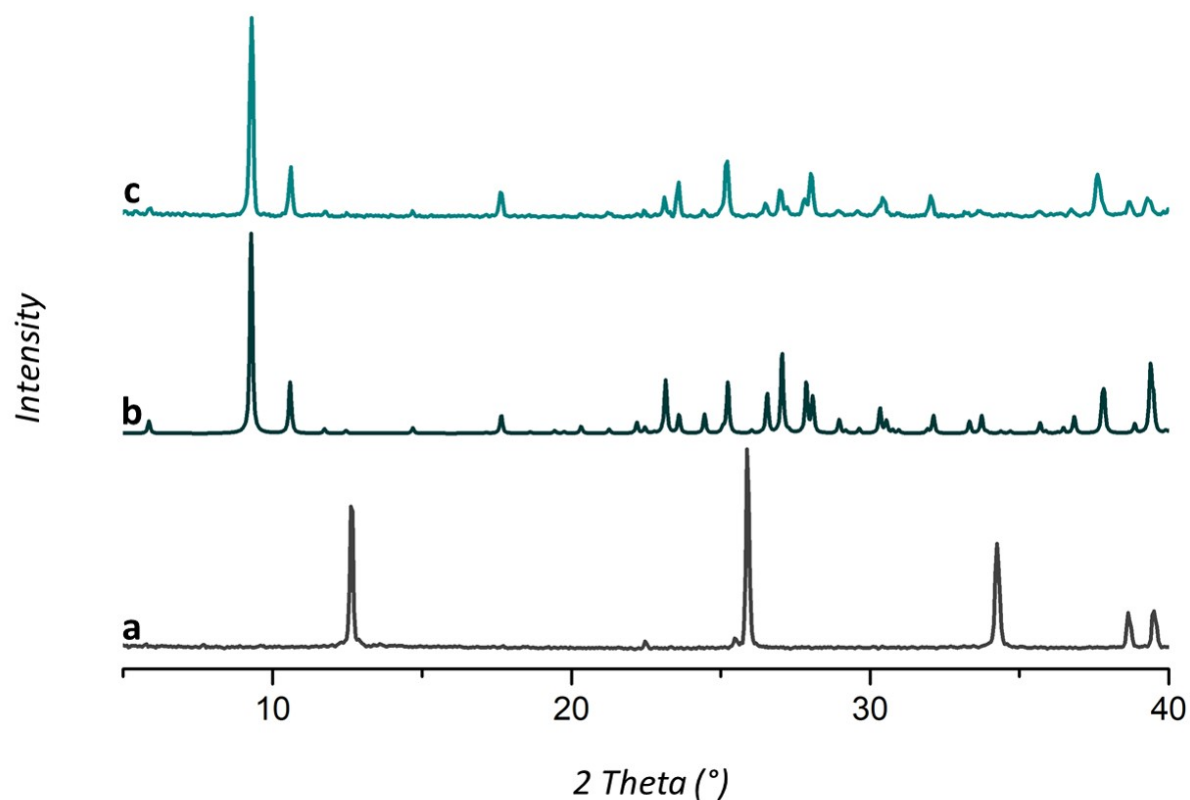
Figure S5. Powder X-ray diffraction patterns: a) experimental pattern of PbI_2 (Sigma Aldrich) b) simulated pattern of $(H_3O)_2Pb_3I_8 \cdot 6H_2O$ (**2**) and c) experimental pattern of the milling product from the PbI_2 :3HI stoichiometric reaction.
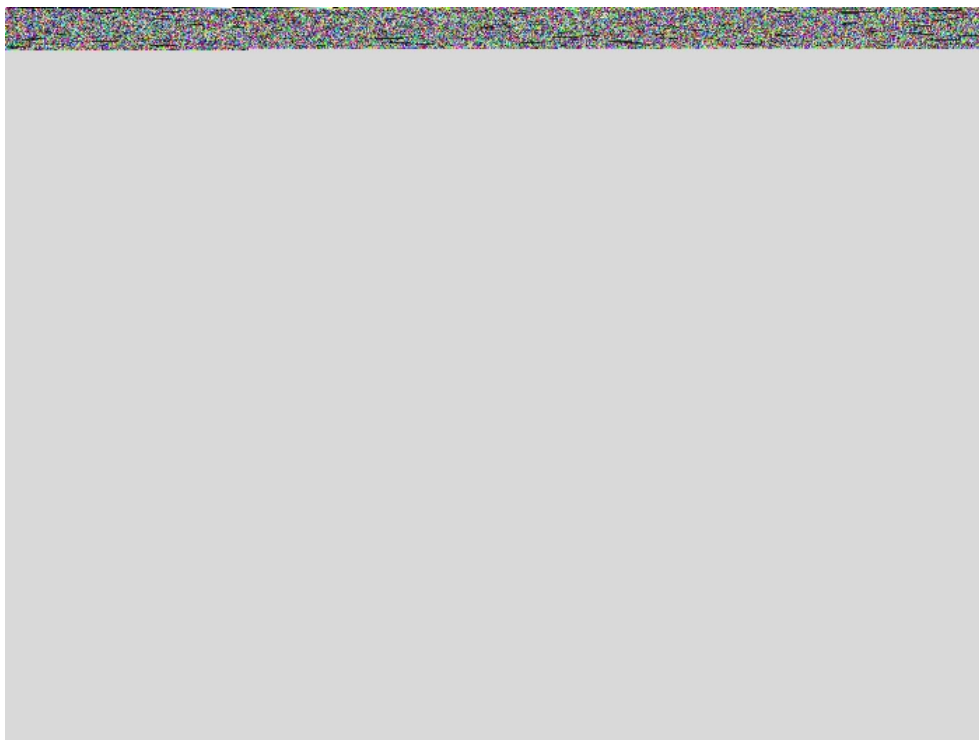
Figure S6. The ORTEP drawing of $(H_3O)_2\text{-}xPb_xI_2\cdot(2\text{-}2x)H_2O$ (**1**) crystal structure collected at ambient pressure.
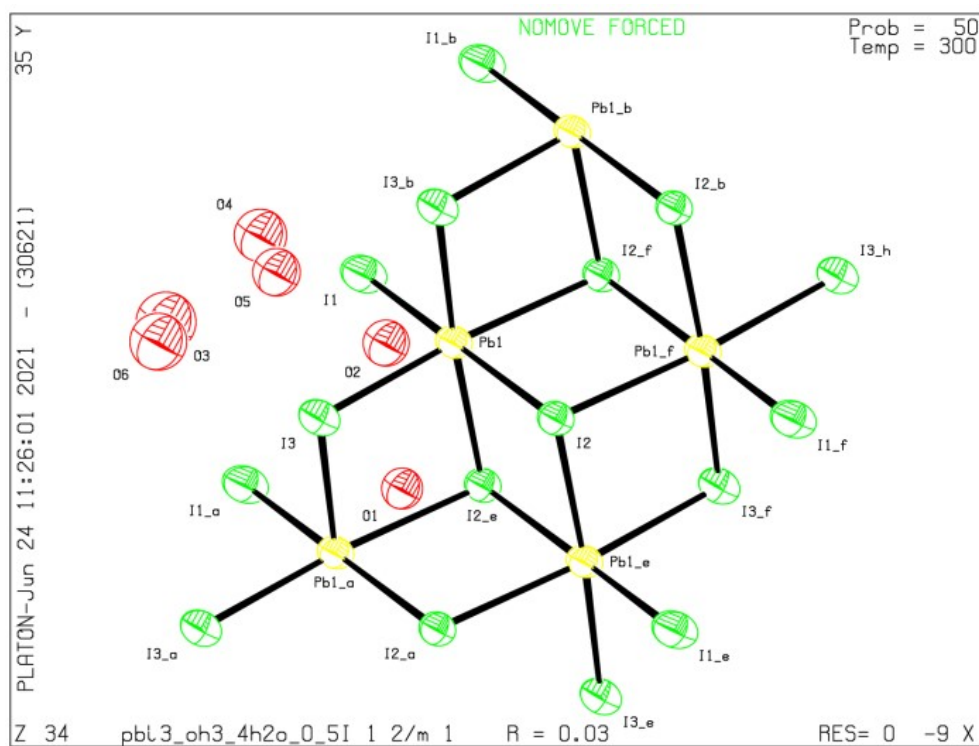
Figure S7. The ORTEP drawing of $(H_3O)PbI_3\cdot4H_2O$ (**3**) crystal structure determined at 0.5 GPa.
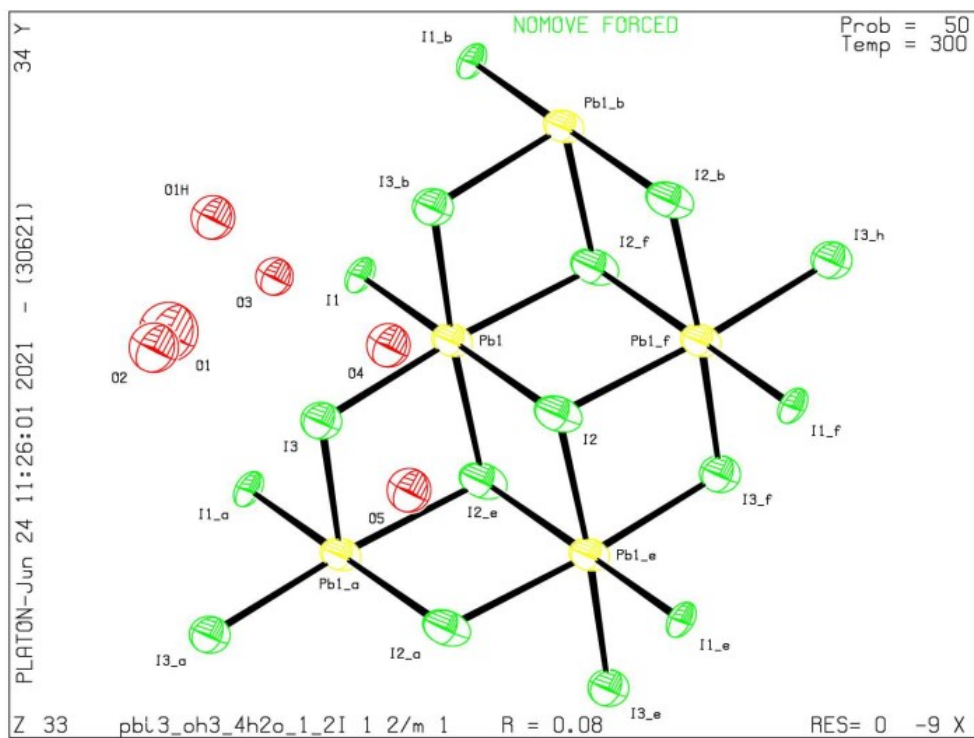
Figure S8. The ORTEP drawing of $(H_3O)PbI_3 \cdot 4H_2O$ (**3**) crystal structure observed at 1.2 GPa.
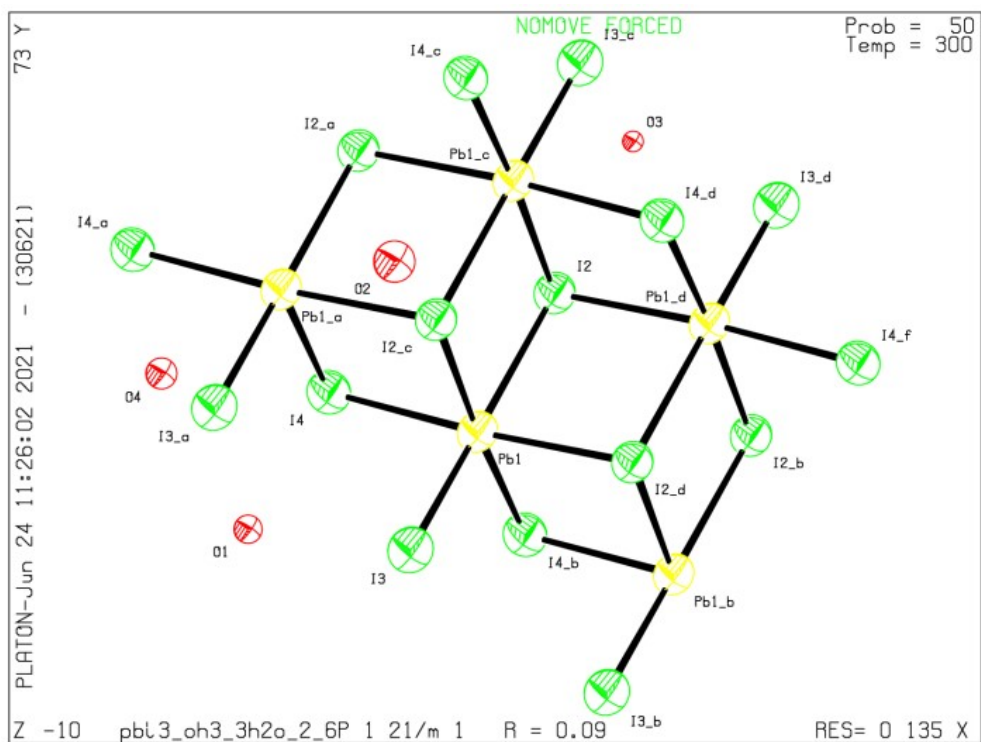
Figure S9. The ORTEP drawing of $(H_3O)PbI_3 \cdot 3H_2O$ (**4**) crystal structure collected at 2.63 GPa
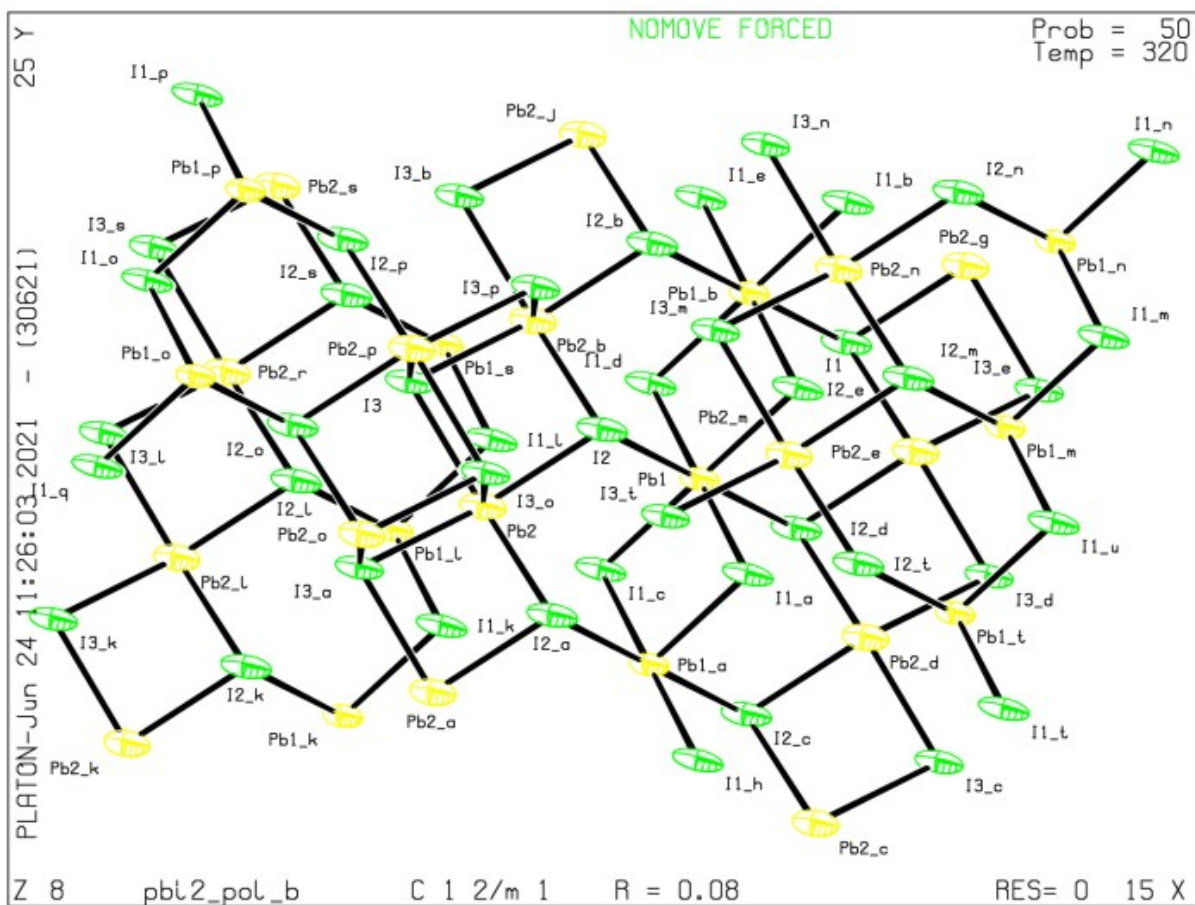
Figure S9. The ORTEP drawing of the β- PbI$_2$ crystal structure obtained at 2.05 GPa.
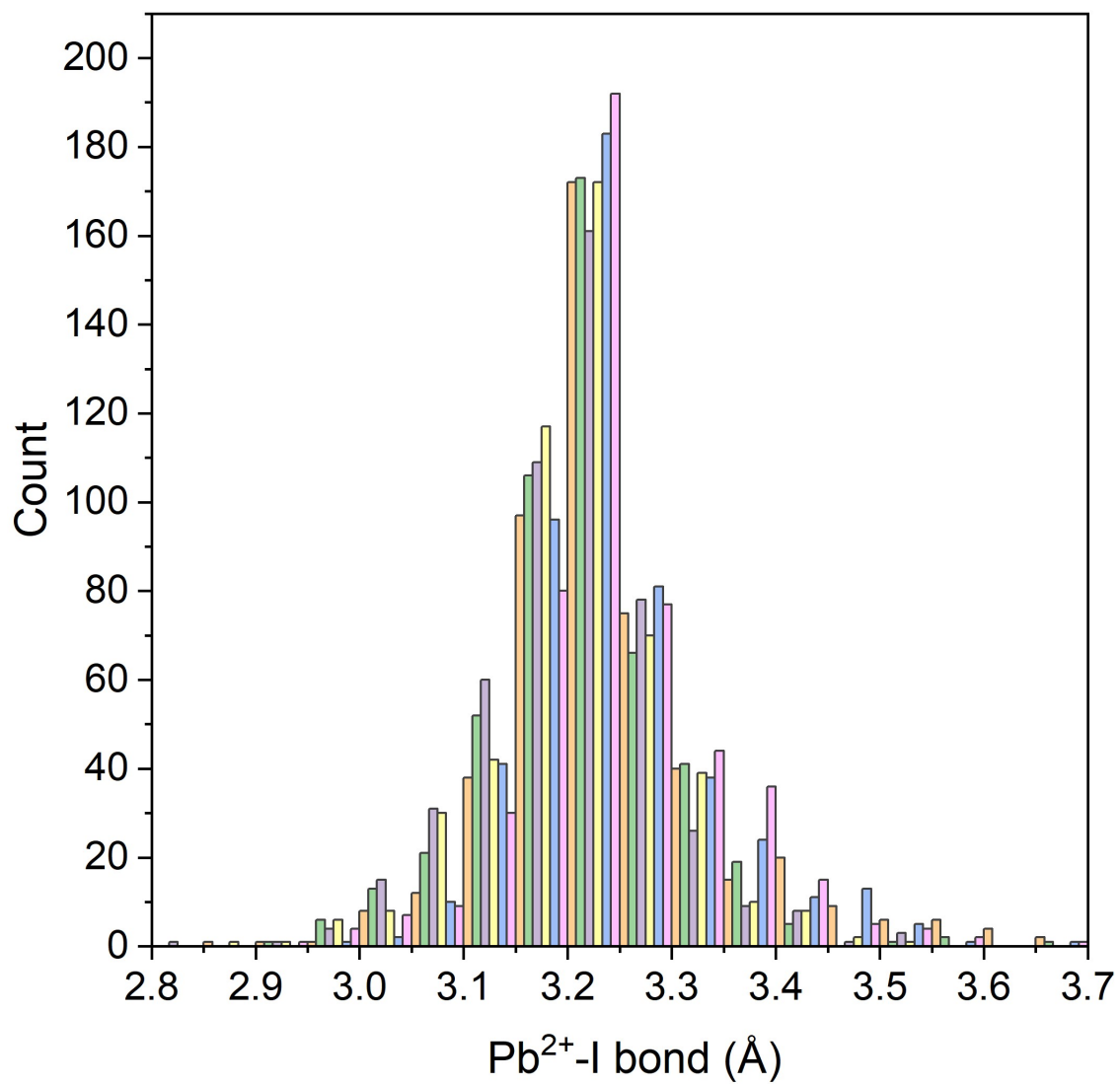
Figure S10. Histogram of Pb(II)–I bond distances in 6-coordinate complexes in crystals deposited in the Cambridge Structural Database (November 2021 release).[11]

References

(1)   Merrill, L.; Bassett, W. A. Miniature Diamond Anvil Pressure Cell for Single Crystal X-Ray Diffraction Studies. *Rev. Sci. Instrum.* **1974**, *45* (2), 290–294. https://doi.org/10.1063/1.1686607.

(2)   Katrusiak, A. High-Pressure Devices. In *International Tables for Crystallography (2019). Vol. H.*; 2019; pp 156–173. https://doi.org/10.1107/97809553602060000942.

(3)   Mao, H. K.; Xu, J.; Bell, P. M. Calibration of the Ruby Pressure Gauge to 800 Kbar under Quasi-Hydrostatic Conditions. *Journal of Geophysical Research*. 1986, pp 4673–4676. https://doi.org/10.1029/jb091ib05p04673.

(4)   Piermarini, G. J.; Block, S.; Barnett, J. D.; Forman, R. A. Calibration of the Pressure Dependence of the R1ruby Fluorescence Line to 195 Kbar. *J. Appl. Phys.* **1975**, *46* (6), 2774–2780. https://doi.org/10.1063/1.321957.

(5)   Budzianowski, A.; Katrusiak, A. High-Pressure Crystallographic Experiments with a CCD-Detector. In *High-Pressure Crystallography*; Springer Netherlands: Dordrecht, 2004; Vol. 140, pp 101–112. https://doi.org/10.1007/978-1-4020-2102-2_7.

(6)   Oxford Diffraction (2004). Oxford Diffraction Ltd., Xcalibur CCD system, CrysAlis Software system, Version 1.171

(7)   Katrusiak, A. Shadowing and Absorption Corrections of Single-Crystal High-Pressure Data. *Zeitschrift für Krist. - Cryst. Mater.* **2004**, *219* (8), 461–467. https://doi.org/10.1524/zkri.219.8.461.38328.

(8)   Sheldrick, G. M. Crystal Structure Refinement with SHELXL. *Acta Crystallogr. Sect. C Struct. Chem.* **2015**, *71* (1), 3–8. https://doi.org/10.1107/S2053229614024218.

(9)   Dolomanov, O. V.; Bourhis, L. J.; Gildea, R. J.; Howard, J. A. K.; Puschmann, H. OLEX2: A Complete Structure Solution, Refinement and Analysis Program. *J. Appl. Crystallogr.* **2009**, *42* (2), 339–341. https://doi.org/10.1107/S0021889808042726.

(10)   Lambrecht, W. R. L.; Limpijumnong, S.; Rashkeev, S. N.; Segall, B. Electronic Band Structure of SiC Polytypes: A Discussion of Theory and Experiment. *Phys. status solidi* **1997**, *202* (1), 5–33. https://doi.org/10.1002/1521-3951(199707)202:1<5::AID-PSSB5>3.0.CO;2-L.

(11)   Groom, C. R.; Bruno, I. J.; Lightfoot, M. P.; Ward, S. C. The Cambridge Structural Database. *Acta Crystallogr. Sect. B Struct. Sci. Cryst. Eng. Mater.* **2016**, 72 (2), 171–179. DOI: 10.1107/S2052520616003954